13th International Symposium on Particle Image Velocimetry – ISPIV 2019
Munich, Germany, July 22-24, 2019

A characterization of the flow around a surface mounted cube by TR-PIV and -3D Shake-The-Box

Andreas Schröder[1,*], Daniel Schanz[1], Reinhard Geisler[1], Tobias Jahn[1], Christian E. Willert[2], Benjamin Leclaire[3], Quentin Gallas[4]

[1]German Aerospace Center (DLR), Department of Experimental Methods, Göttingen, Germany

[2]German Aerospace Center (DLR), Department of Engine Measurement Systems, Cologne, Germany

[3]DAAA, ONERA, University Paris Saclay, F-92190 Meudon, France

[4]Univ. Lille, CNRS, ONERA, Arts et Metiers Paris Tech, Centrale Lille, FRE 2017 LMFL - Laboratory of Fluid Mechanics of Lille - Kampé de Fériet, F-59000, Lille, France

*andreas.schroeder@dlr.de

Abstract

The flow around a surface mounted cube with incoming turbulent boundary layer has been topic of many experimental and numerical investigations in the past decades. Despite its simple geometry the flow generates a set of complex vortical structures, includes flow separation at the three front plane edges with corresponding subsequent shear layer dynamics and recirculation zones and organizes a large unsteady flow separation region downstream of the cube which is associated with typical quasi-periodic bluff-body wake dynamics. Because of its generic role for geometry induced flow separation and its complex unsteady vortical properties the flow around a surface mounted cube is often used for bench-marking purposes to validate turbulence models and advanced numerical methods, while an increasing interest of DNS investigations in the recent years including the laminar boundary layer flow case can be registered. Furthermore, the flow configuration is well suited to enhance the understanding of similar unsteady and separated flow phenomena in many aerodynamic and engineering applications. In the present experimental investigation we aim at resolving a large spectrum of spatial and temporal scales in the flow around a cube with incoming laminar and turbulent boundary layers by using the most recent developments of 3D Lagrangian Particle Tracking (LPT) and high resolution TR-PIV. The results are partly documented in the present paper and consist of long time-series of highly resolved 3D and 2D velocity fields as well as unsteady 3D pressure volumes allowing for the analysis of coherent structure dynamics and of corresponding statistical Lagrangian and Eulerian flow properties.

1 Introduction

In the last few decades, there has been extensive research on turbulent boundary layer (TBL) and turbulent channel flows around wall-attached obstacles including cubes with various aspect ratios roughly in the range of $H/\delta \sim 0.2$ to 4 resp. $H/h \sim 0.1$ to 0.3 (where H is the obstacle or cube height, δ accounts for the boundary layer thickness and h for the channel height). However, in the first group of investigations mainly the case with high Reynolds numbers (Re_H >10,000) and incoming TBL flows has been addressed (e.g. mimicking buildings in atmospheric BL) with the aim of identifying the general flow features around the cube. Extensive experimental studies have been performed by Castro and Robins (1977), Martinuzzi and Tropea (1993) and Meinders et al. (1999) all focusing on unsteady pressure distributions and wall-shear stress visualizations using oil-film techniques or similar in order to gain insights into the mean 3D flow structures around and in the wake of the cube using assumptions governed by topological concepts. Hussein and Martinuzzi (1995) generated a detailed velocity vector

map in several planes and locations around the cube using one-point LDA measurements in order to investigate the budget balance of the turbulent kinetic energy transport by mean and fluctuation velocity statistics. Near-surface PIV results of the flat plate around and at the walls of the cube itself by Depardon et al. (2005) allow quantifying the related skinfriction vector fields with identification of locations of mean separation lines, foci- and saddle-point topologies, which was restricted to qualitative visualizations before.

On the other hand extensive numerical simulations using advanced methods like URANS (Iaccarino et al. (2003)) or LES (Krajnovic and Davidson (2002), Lim et al (2009), the latter combined with experiments) at relatively high and DNS at lower Reynolds numbers (Yakhot et al. (2006a,b), Diaz-Daniel et al. (2017)) enables an analysis of the unsteady behavior of 3D coherent flow structures which in the past have been identified often only partly and in a mean sense. These structures with characteristic dynamics depending on the governing conditions within the specific flow regions around the cube have been topic of individual research interest. Lim et al. (2009) focused their investigations mainly on the flow, shear layers and recirculation regions above and aside the three streamwise cube surfaces. In the work of Yakhot (2006a) the unsteadiness of the vortical structures and induced bimodal vertical velocity distribution in front of the cube which are the origins of the well-known horseshoe vortices surrounding the cube in the near wall region was the main focus of investigation. Diaz-Daniel et al. (2017) extensive DNS work of the flow around a cube with incoming turbulent and several laminar boundary layer flows at six different low Reynolds numbers enables the investigation of the specific dynamics of the shear layers, horse-shoe vortices and wake flows in direct comparison. They showed that the laminar flow case features specific wake dynamics with distinct peaks in several Strouhal numbers when transitional shear layers, the stability of the horse-shoe vortex and hair-pin vortices interfere in the wake with the overall flow topologies of the separated flow region depending on increasing Reynolds numbers. This work is the closest numerical research case when compared to the parameters of the present experimental study concerning the choice of flow configurations. Although for the majority of flow cases the DNS was performed at slightly lower Reynolds numbers than in our present experimental investigation, many features quantified by the present flow measurements are very similar and can be compared directly.

In order to catch-up with the recent DNS capabilities enabling the flow simulation of all temporal and spatial scales at least for low Reynolds number flows we applied the novel dense LPT technique Shake-The-Box (STB) (Schanz et al. (2016)) with subsequent data assimilation by FlowFit (Gesemann et al. 2016) and the high resolution TR-PIV technique (Willert (2015)) to the same flow configuration in the water flow facility THBV at ONERA, Lille. The acquired long time-series of particle images comprise of spectral and topological flow information as well as of unsteady 3D and 2D velocity vector and pressure data for converged Lagrangian and Eulerian statistical analysis when evaluated and post-processed properly. The LPT and (with limitations) the TR-PIV techniques can in principle be adapted to flows with much higher Reynolds numbers and flow speeds not reachable with DNS capabilities within the next few decades, while still a very high dynamic temporal and spatial range at least for one-point statistics of the velocity fields and Lagrangian tracks can be reached e.g. in small fields of view (see Beresh et al. (2017)) or by multi-pulse STB (see Novara et al. (2016) (2019)). For example, in compressible and swept wing aerodynamics there is further research interest in the laminar-transitional flow case when the surface mounted obstacle heights H are much smaller than the BL thicknesses δ thus mimicking surface imperfections and roughness caused by limited manufacturing schemes in aerodynamic vehicle production. These surface imperfections in the µm-range lead to modal and non-modal growth of the induced disturbances and then to (premature) boundary layer transition during flight. Transitional flow with growing tiny disturbances in thin boundary layers around wings in transonic wind speeds is nowadays reachable for micro 3D LPT based advanced optical measurement methods.

The next chapter describes the experimental set-up of the TR-PIV and 3D LPT measurement systems at the THBV water flow facility in Lille and the related specific calibration and evaluation schemes. From the upstream TR-PIV measurement a detailed quantification of the incoming BL flow properties has been realized (see as well Chapter 2). In Chapter 3 exemplary instantaneous and mean flow results of TR-PIV

and 3D STB measurements are shown. Further post-processing and analysis options are explained and described. In the last chapter we conclude with a list of the gained results and a short outlook.

2 Experimental set-up

2.1. TR 2D2C-PIV

The following provides an overview of the boundary layer profile measurements obtained upstream of and around a surface mounted cube of 10 mm height H in the center plane with high resolution TR-PIV at the THBV water flow facility in Lille. The measurement configurations and the used experimental hardware are described. A variety of results are provided to illustrate the overall quality of the acquired data and demonstrate some of the possible post-processing methods. The PIV measurement approach employed in these experiments closely follows the procedures and methods laid out in the paper by Willert (2015). The near-wall measurement approach has been successfully used in a variety of previous applications, such as for turbulent boundary layer measurements with zero and adverse pressure gradients. The imaging setup was designed for a magnification of m = 0.66 using a macroscopic lens of 100 mm focal length (*Zeiss-Planar T 100/2*) at an aperture of f-number 4.0. On the imaging side a high-speed camera with a 4 megapixel (4 MP) CMOS sensor was used (*PCO AG, DIMAX-S4*, which has a pixel pitch of 11 µm corresponding to 16.67 µm/pixel in object space (set-up at THBV see Fig. 1). Using macroscopic imaging the smallest viscous scales anticipated at the design point of $U_\infty \approx 0.8$ m/s with $Re_T = 400$ and $Re_\theta = 1000$ amounted to about 28 µm per wall unit (y^+) and could be resolved with nearly single pixel resolution. For the upstream boundary layer measurements the field of view of the camera was reduced to 240 pixel width and 1008 pixel in height (4.0×16.7 mm²). This reduction allowed an increase of the number of acquired images to more than 100,000 during a single run. The roughly 5-10 mm wide measurement area was illuminated by a pair of externally modulated continuous wave lasers (*Kvant Laser, SK*) with a combined output power of nearly 10 W at a wavelength of 520 nm. Focusing lenses narrowed the light sheet to a thickness of about 200-300 µm in the measurement area. Synchronization between modulated laser and high-speed camera was provided through a separate signal pulser unit (*Arduino MEGA 2560*).

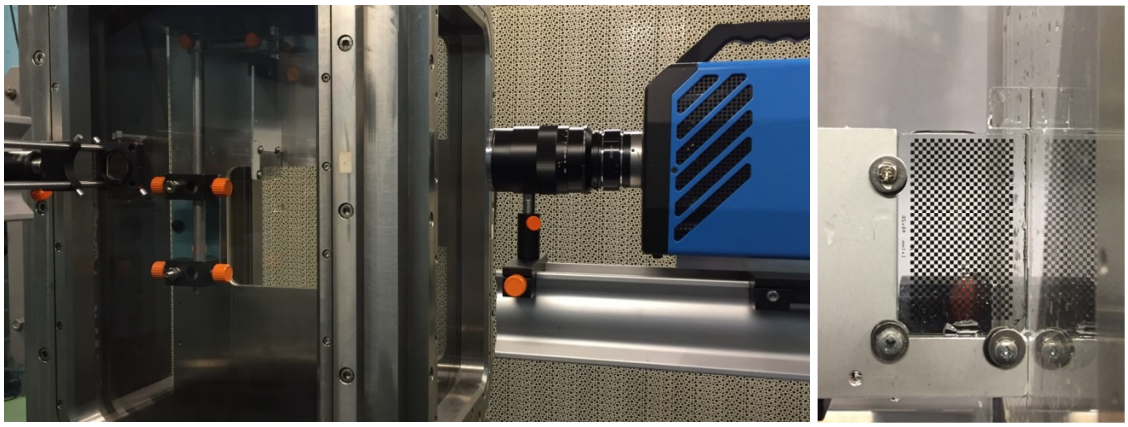

Figure 1: High resolution TR-PIV setup to image the upstream area of the cube. The calibration target can be seen installed upstream of the cube (left) and calibration target placed downstream of the cube (right)

2.2. Configurations: Incoming laminar and turbulent boundary layer flows

For all four measurement locations data was acquired for the tripped, turbulent boundary layer case ($U_\infty = 0.8$ m/s at $Re_\theta = 1000$) and the four laminar BL cases ($U_\infty = 0.2, 0.4, 0.6, 0.8$ m/s) corresponding to $Re_H = [2000, 4000, 6000 \text{ and } 8000]$ with H = 10 mm and H/δ aspect ratios as indicated in Table 1.

2.3. Analysis

The TR-PIV image sequences were processed using a conventional 2C-2D cross-correlation PIV processing algorithm, using a coarse-to-fine pyramid approach with intermediate validation (normalized median filter and smoothing), the final interrogation window size is 64×6 pixels (1070 ×100 µm²) for the upstream boundary layer characterization and 16×16 pixels (270×270 µm²) for the other three imaged areas. Sampling distances were approximately 30% of the sample size. For the upstream measurement position a large aspect ratio was chosen to achieve optimal wall-normal spatial resolution in the recovered velocity profiles.
To normalize the averaged velocity data, a fit to DNS data from Schlatter et al. (2009) in the range of $10^+ < y < 200^+$ yielded the necessary wall shear stress estimate. Subsequent analysis using single pixel-line processing using the methodology proposed in Willert (2015) yield a further estimate of the wall shear rate (and shear stress). The relevant boundary layer parameters of the upstream position at x= -4.2H are summarized in Table 1. Compared to the best-fit to the DNS data the wall-shear rate measurement is underestimated by about 5% which can be attributed to a bias of the estimated near wall velocity toward zero. More advanced processing algorithms (for a comparison of TR-PIV with 2D STB techniques see Schröder et al. (2018)) are required here to properly reject erroneous near-wall measurement data. The mean velocity profiles obtained by processing individual sequences of nearly one minute duration acquired at 2 kHz are presented in Fig. 2 (left) for both laminar and turbulent cases. Normalization was done by the outer velocity U_e and the 99-percentile boundary layer thickness δ_{99}.
The turbulent velocity profile normalized with inner (viscous) variables is presented in Fig. 2 (right) together with DNS data provided by Schlatter et al. (2009). Deviations from the linear profile of the viscous sublayer can be attributed to the spatial filtering effect of the finite sampling window height (6 pixel = 100 µm). Corresponding profiles of the fluctuation of the stream-wise velocity $\langle u^+u^+\rangle$, the wall-normal velocity $\langle v^+v^+\rangle$ and co-variances $\langle u^+v^+\rangle$ have been calculated as well (not shown here), but the reduced spatial resolution near the wall introduces measurement noise left of the inner turbulence peak at $y^+ = 13.5$. Compared to the DNS data the wall-normal fluctuations $\langle v^+v^+\rangle$ seem to be underestimated mainly due to the large correlation window size in flow direction of 64 pixel corresponding to 1.07 mm.

Condition	**-**	**turb.**	**laminar**	**laminar**	**laminar**	**laminar**
Tunnel setting, U_∞	m/s	0.8	0.8	0.6	0.4	0.2
Measured U_e	m/s	0.829	0.830	0.628	0.419	0.210
BL-thickness, δ_{99}	mm	11.22	4.18	4.70	5.58	7.57
Displ. thickn., δ^*	mm	1.80	1.45	1.63	1.90	2.58
Momentum thickn., θ	mm	1.23	0.55	0.61	0.71	0.98
Shape factor, $H=\delta^*/\theta$	-	1.46	2.66	2.68	2.66	2.64
Friction coeff., cf	-	0.00441	-	-	-	-
Meas. wall shear rate	1/s	1394	-	-	-	-
Estim. wall shear rate	1/s	1430	-	-	-	-
Estim. friction vel, u_τ	m/s	0.0389	-	-	-	-
Viscous length, y+	µm	27.2	-	-	-	-
pixel / wall unit	-	1.64	-	-	-	-
Re_δ	-	8780	3320	2760	2190	1440
Re_θ	-	966	428	359	283	194
Re_τ	-	412	-	-	-	-

Table 1: Characteristic parameters of the boundary layer at upstream position, x = -4.2H (Pos.1)

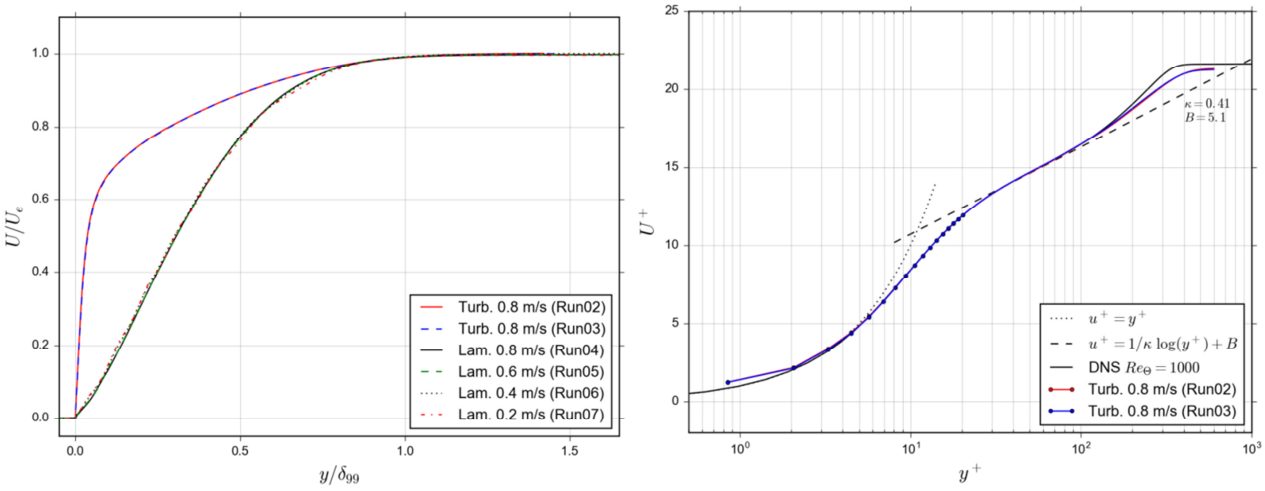

Figure 2: Mean velocity profiles at x = -4.2H upstream of the cube scaled with outer velocity U_e and boundary layer thickness δ_{99} (left) Velocity profile for turbulent case at x=-4.2H upstream of the cube normalized with inner (viscous) variables. For clarity symbols are only shown for $y^+ < 20$ (right)

2.4. 3D-STB experimental set-up

The boundary layer flow around a glass cube with 10 mm edge length and height H mounted on a flat plate with glass insert was investigated with the time-resolved 3D-STB technique enabling dense Lagrangian particle tracking in the measurement volume. In total seven high-speed cameras and a high repetition laser for volume illumination (see Fig. 3 and 4) has been used to carry out the experiment in a water flow of the THBV at ONERA, Lille. The different boundary layer flow conditions are chosen as qualified by TR-PIV and reported above. The full measurement matrix with specific relevant acquisition parameters is given in Table 2. Both flow cases are of eminent interest for the understanding of complex geometry induced flow separation with transitional and turbulent shear and wake development regions.

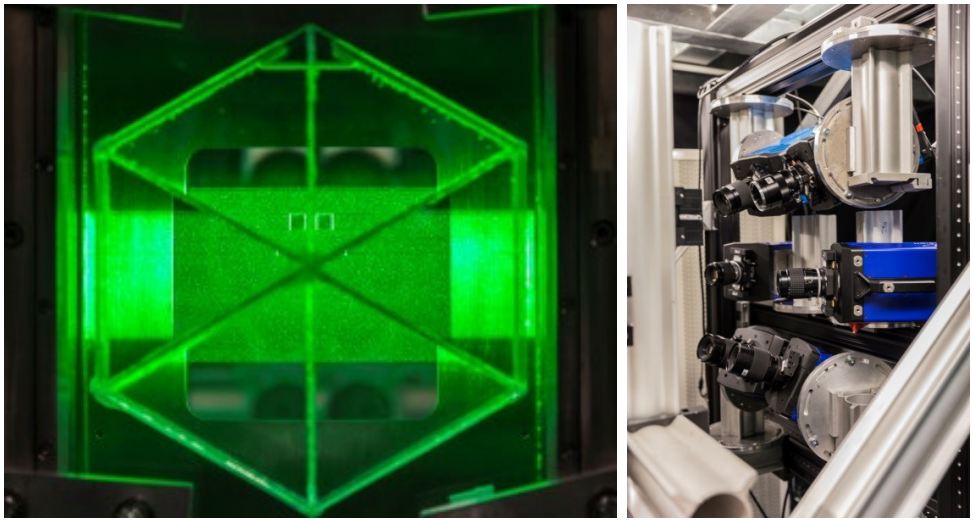

Figure 3: Laser volume illumination of particles in the flow around the surface mounted glass cube (view through six-folded prism) (left) and six high-speed cameras viewing at measurement volume (right). A seventh camera viewed from the backside. Images taken at THBV at ONERA in Lille.

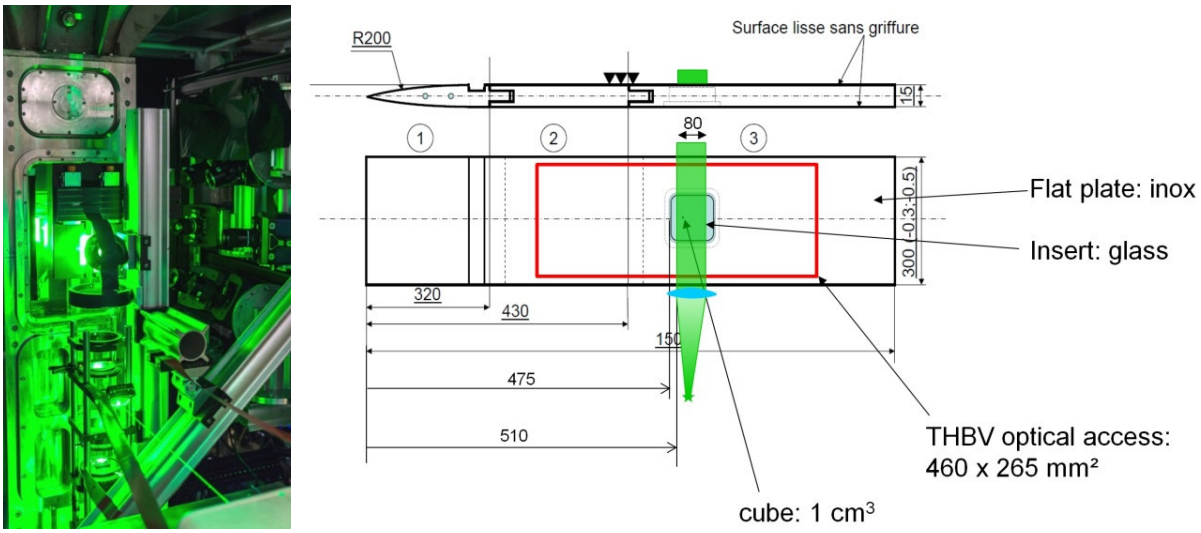

Figure 4: Overview of the experimental setup with light-sheet optics attached to the tunnel and camera system in the back (left) and sketch of the flat splitting plate with elliptical leading edge and the location of the cube and the measurement volume in the water tunnel (right)

Condition		**Laminar**	**Laminar**	**Laminar**	**Laminar**	**Turbulent**	**Turbulent, no cube**
Tunnel setting, U_∞	[m/s]	0.8	0.6	0.4	0.2	0.8	0.8
Acquisition frequency	[Hz]	1,500	1,125	750	375	1,500	1,500
Total number of images		29,400	22,050	22,044	22,044	55,125	14,700

Table 2: Measurement matrix for the volumetric 3D STB experiment

A hexagonal prism was installed at the front glass window of the water tunnel in order to realize nearly orthogonal viewing conditions through the air-glass-water interfaces for each camera avoiding astigmatism effects for particle imaging. In order to capture the flow in an extended volume around the cube in full time-resolution, a system of seven high-speed cameras (6 x *PCO.Dimax* @ 4 MP + 1 x *Phantom Miro* reduced to ~2 MP) was set up, while the six *PCO* cameras viewed with different nearly symmetric viewing angles through the prism attached to the water tunnel front glass and the seventh *Phantom Miro* camera viewed through the backside glass with a high-magnification factor around the immediate vicinity of the cube covering only a small fraction of the overall volume, but acquiring complementary images of the cube induced "shadow" regions of the other six camera lines-of-sight. A high-repetition laser system (*Quantronix Darwin Duo* with 20 mJ pulse energy at 1kHz) was used to illuminate a rectangular section of approx. 80 mm in streamwise direction and 20 mm in wall-normal direction using beam shaping optics and a passe-partout, while the collimated laser beam was back reflected through the measurement volume (see Fig. 3 and 4). The common field of view of the camera system covered a section of approx. 70 mm in spanwise direction. The six *PCO* cameras were equipped with f=100 mm *Zeiss Makro-Planar* lenses while the Phantom camera was equipped with a f = 200 mm *Nikon Makro* lens.

2.5. Challenges in STB particle tracking for the 3D cube flow experiment

For the specific challenges faced during the calibration of the 3D STB system and subsequent evaluation of particle images several improvements on top of the existing time-resolved Lagrangian particle tracking

code have been implemented and tested. First the calibration and volume matching of the seventh camera view with a much smaller field of view and higher magnification factor has been adapted. Starting with the calibration target the number of visible markers in the seventh camera was too low in order to realize a common volumetric calibration together with the common view of the other six cameras. Therefore, as first indicator the cube edges have been detected in the field of view. Then the commonly viewed particles were used to iteratively match the existing calibration of the six cameras onto the smaller volume in the sight of the seventh camera. Then for all cameras a local determination of the particles optical transfer function (OTF) has been realized according to Schanz et al. (2012), right after VSC (Wieneke (2008)).
In a second challenge a volumetric mask has been created in order to take into account that the cube is located within the measurement volume and thus within the individual cameras lines-of-sight. Although the cube was made of glass (necessary for the volumetric, collimated and back-reflected laser illumination) the refractive index is sufficiently different compared to water so that particles detected "behind" the cube with respect to each single camera line-of-sights need to be ignored as part of the STB evaluation steps. Those particles undergo a massive image shift viewed through the cube glass surfaces under different angles. Nevertheless, with all seven cameras it was possible to see all areas around the cube with at least three cameras.
The procedure for the 3D mask just applies a virtual 2D mask on each camera image covering the top surface of the cube. Then each camera is not used for particles which are located below z = 10 mm in height and where the projection point lies within 2D mask. The geometrical set-up for a single camera using each a 2D mask is explained in Figure 5 left and right.

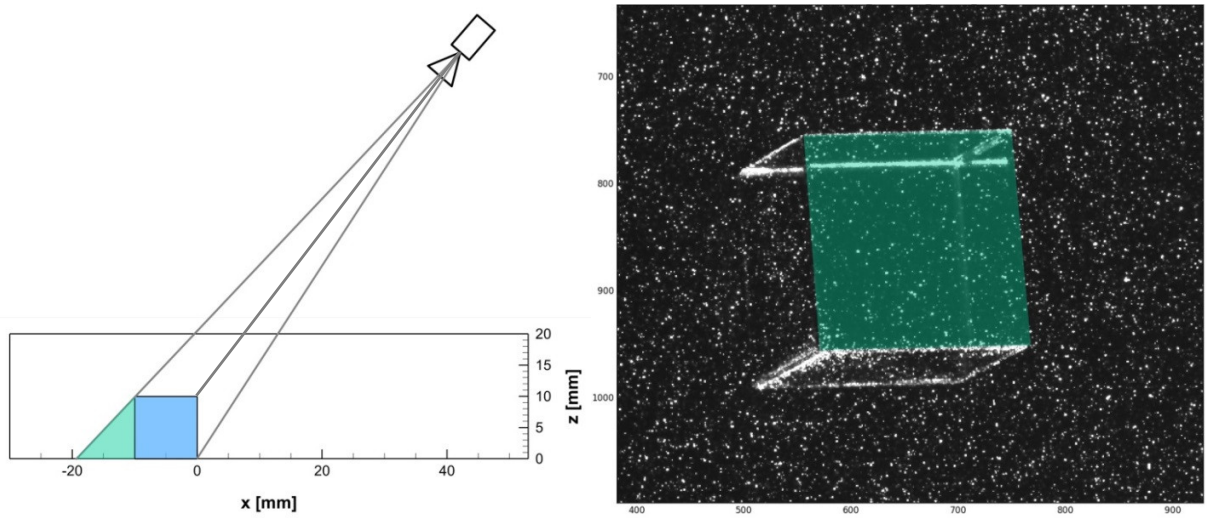

Figure 5: Single camera viewing of the cube (left) and applied 2D mask on top cube surface at a particle image and using the condition to ignore particle images below z = 10 mm height in the projection area behind the mask (left and right)

The used polyamide seeding particles from *Vestosint* induced an unfavorable very high dynamic intensity range with a corresponding unpleasant variation of the particle image diameters between two and eight pixels. These particles are quite polydisperse, having a large variation of shapes and diameters between ~5 µm and 80 µm with a central peak at the average diameter of ~30 µm. For future investigations in such large water facilities we would recommend e.g. less polydisperse and low-cost *Orgasol* polyamide particles. Further on, STB evaluation challenges were connected to the fact that the flow is highly turbulent and three-dimensional and very strong shear regions are present above the geometry-induced flow separations starting at the front side edges of the cube. At the strong shear layers a predictor from neighboring particles was not reliable. Furthermore, strong acceleration events of particles along trajectories around these side edges and in the wake of the cube occur, leading to less accurate particle position predictions for the next time step and subsequently an increased loss of tracks in these regions.

Additionally high grey values in the background image from the light scattered at the cube edges complicate the evaluation situation of particle tracks close to the edge positions. To overcome some of the difficulties related to these regions and high acceleration events we used averaged 3D flow field results from preliminary STB evaluations as predictor by: a) Using velocity information as predictor for finding new tracks, b) Parametrize RMS values componentwise as search radius and c) Using both as outlier filter for running tracks. These additional schemes included in the STB evaluation enable a robust and reliable 3D Lagrangian particle tracking in the full volume.

2.6. FlowFit: Navier-Stokes regularized interpolation to a Cartesian coordinate system

After fitting the found particle tracks temporally by third-order B-Splines with an optimized parametrization from a spectral analysis (TrackFit) (Gesemann et al. (2016)) we gain all particle positions, velocities and accelerations in a scattered manner within our 3D measurement volume by analytical differentiation. In order to get the full time-resolved 3D velocity field and velocity and acceleration gradient tensor we further calculate an interpolation of the scattered particle information onto a continuous flow field representation by fitting a system of uniform 3D B-splines to the given scattered discrete velocity and acceleration values. This is done by applying a fully incompressible Navier-Stokes regularization which is imposed onto the grid of B-Splines by optimizing iteratively a set of related cost functions using a non-linear optimization algorithm (here LBFGS). The related cost functions are weighted according to the measurement noise and are penalizing curvature, div u, div du/dt and the differences between measurements and interpolations at particle locations (Gesemann et al. (2016)). FlowFit avoids the classical correlation-window-based low-pass filtering (known from Tomo PIV), increases the spatial resolution by following the imposed physical constraints (data assimilation) and allows for an arbitrary sampling on desired grids as well for derivations which can be directly computed on any position from the continuous functions (like Vorticity, Q-criterion,…).

3 Results

3.1. Time-resolved PIV for 2D2C velocity fields

3.1.1. Measurement positions

The four measurement positions chosen for the high-resolution 2C-2D TR-PIV measurements are shown in Fig. 6 with one location about 42 mm upstream of the cube (x = -4.2H) for boundary layer flow characterization. Pos. 3 was centred at 1.5H downstream of the cube. Position 2 mapped the area above the cube while Position 4 mapped the stagnation zone upstream of the cube. All measurement areas are aligned with the centreline (z=0) of the plate and cube. The reference point of the coordinate system is placed on the upstream side of the cube, with X aligned in stream-wise direction pointing in flow direction, Y in wall-normal direction with y=0 on the flat plate and Z in span-wise direction. Definition of coordinate system origin: X_0 → upstream of cube front face, Y_0 → flat plate wall and Z_0 → middle of cube.

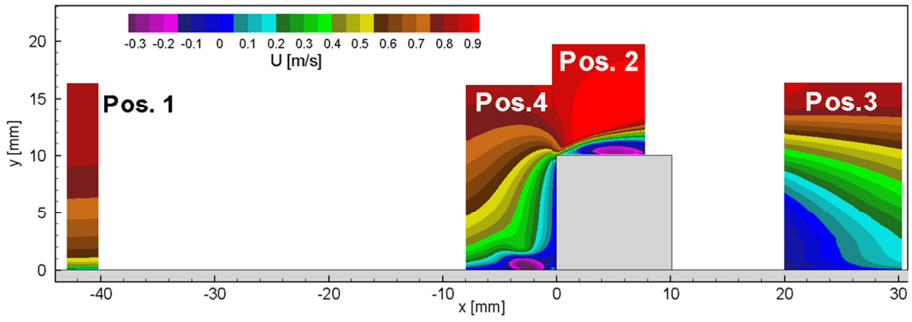

Figure 6: TR-PIV measurement positions

3.1.2. Flow field around the cube at center plane

The following figures provide some exemplary information of the flow around the cube at U_∞ = 0.8 m/s.

Turbulent case, U_∞ = 0.8 m/s | Laminar case, U_∞ = 0.8 m/s

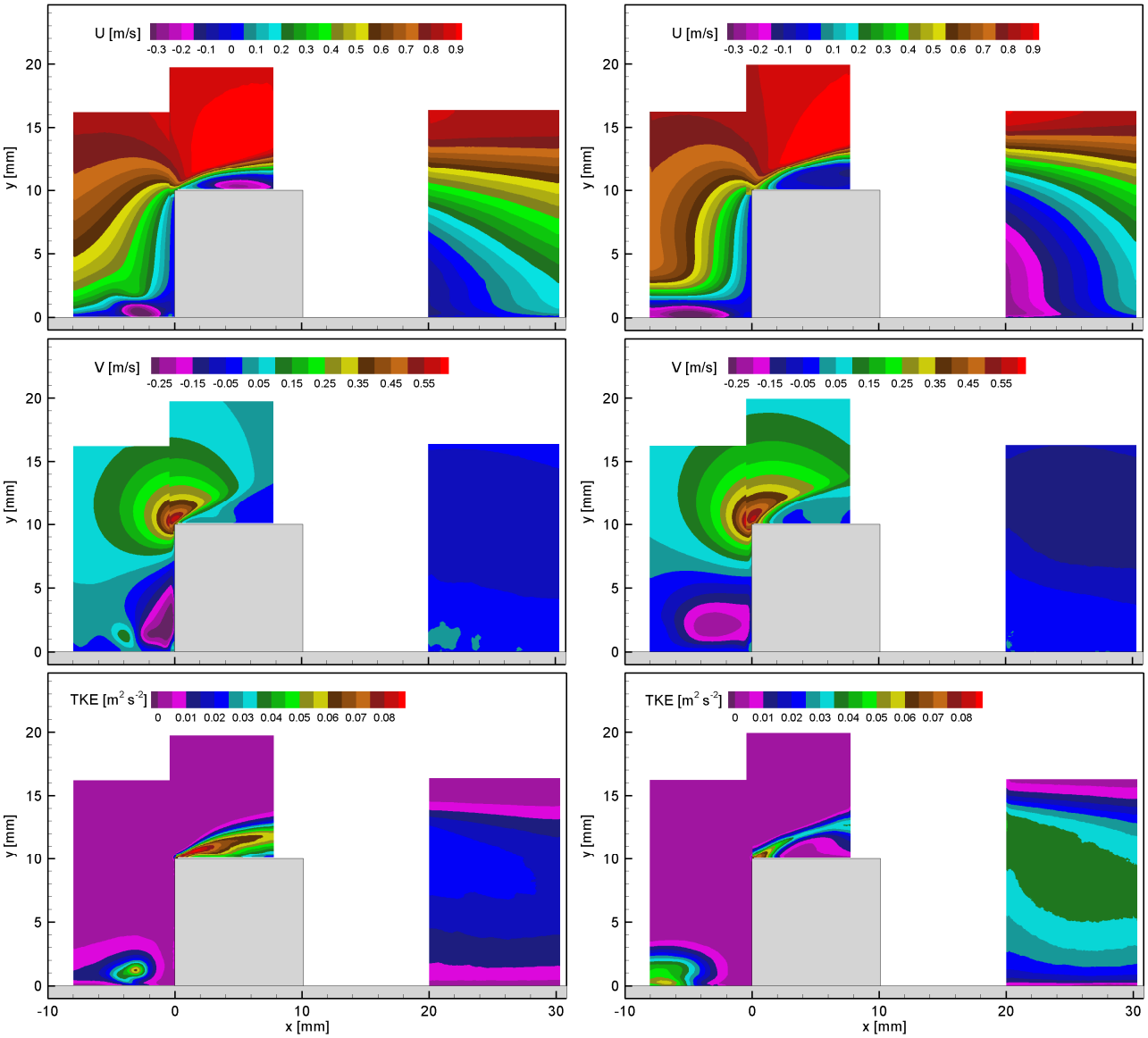

Figure 7: Flow field a center plane (z=0) around cube, turbulent case (left) and laminar case (right), both at U_∞=0.8m/s, mean u- velocity U (top), mean v- velocity (middle), turbulent kinetic energy (bottom)

In Fig. 7 interesting flow features can be detected: For the turbulent flow case with δ/H = 1.12 the mean reattachment point downstream of the flow separation in the cube wake is at x = 2.5 H, while it is more downstream at x = 2.8 H for the laminar case with δ/H = 0.42. Furthermore, the separation bubble size on top of the cube is higher in y-direction for the laminar case induced by stronger flow curvature due to the lower boundary layer thickness. On the other hand, the turbulent flow case exhibits larger TKE values in the cubes shear layer on top of the flow separation, but almost twice as low values in the wake region compared to the laminar one. A distinct point of high TKE is visible upstream of the cube close to the wall

for the turbulent case which can be identified as the point upstream of the first-order horse-shoe vortex origin. Here a dynamic bi-modal vertical velocity PDF has been investigated by Yakhot et al. (2006a).
The differences between the TKE values in the cube wake for the two boundary layer flow types can be visualized as well by the two corresponding time traces of the u- and v-velocity profiles at the position of the mean reattachment point for the turbulent case x = 2.5H. Here, a more rapid dynamic of u- and specifically of small scale v-velocity events with strong positive and negative wall-normal values can be recognized in the laminar BL case in Fig. 9 compared to a less pronounced and spatially smoother wake dynamics of the turbulent BL case in Fig. 8. Note as well the different sample length in the time axis.

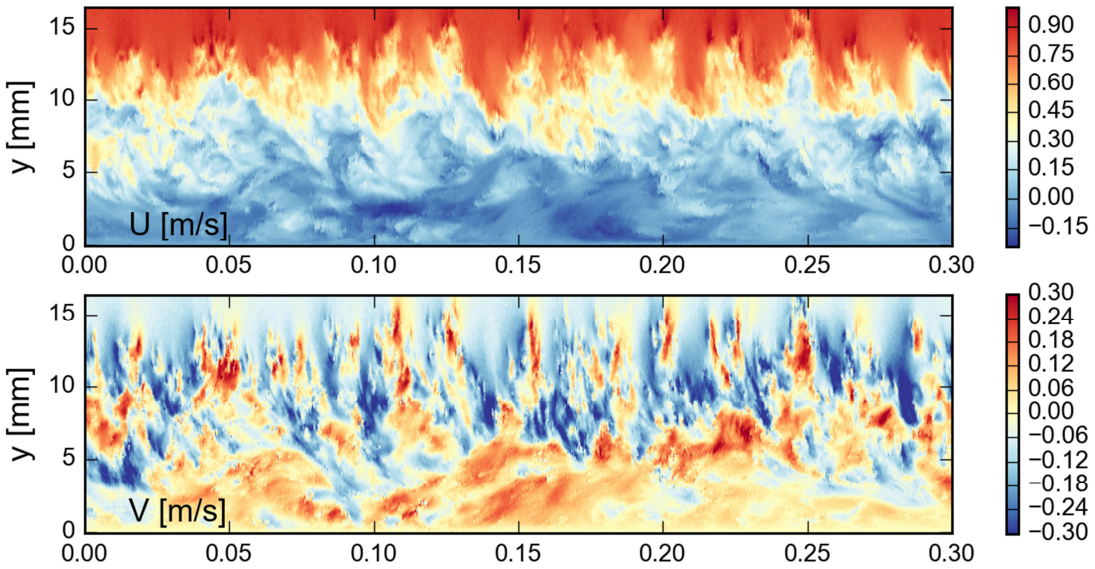

Figure 8: Portion of velocity time record (1000 samples) of turbulent case (Pos3) downstream the cube at x = 2.5D showing stream-wise velocity (top), wall-normal velocity (bottom) in the wake region

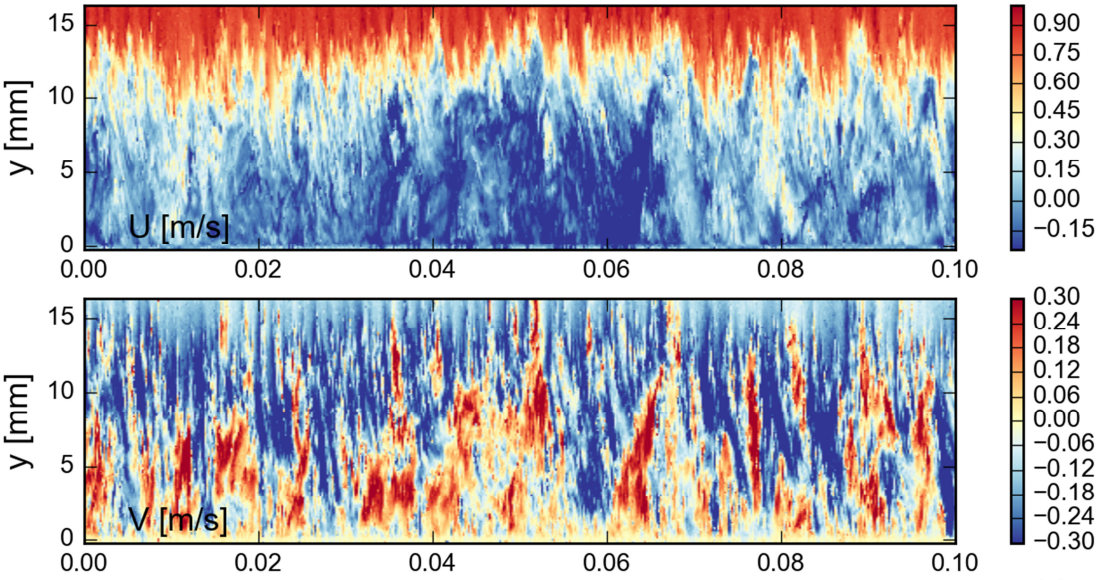

Figure 9: Portion of velocity time record (500 samples) of laminar case (Pos3) behind the cube at x = 2.5D showing stream-wise velocity (top), wall-normal velocity (bottom) in the wake region

3.2. Instantaneous time-resolved 3D3C velocity and acceleration fields

Evaluation of the whole volumetric data set given in Table 1 was performed successfully using Lagrangian Particle Tracking by the Shake-The-Box algorithm (Schanz et al. (2016)). Figure 10 and Figure 11 show exemplary results from a case with laminar inflow conditions at U_∞ = 0.4 m/s. Around 70,000 particles have been instantaneously tracked and the velocity and acceleration resp. material derivative information has been computed directly from the continuous temporal B-spline fit function (TrackFit). 22,050 successive images at a recording frequency of 750 Hz are available for this case (see Table 1).
Figure 10, left shows particle tracks close to the wall (tracks within a slice below y = 1.2 mm) color coded by streamwise velocity. On Figure 10 right at U_∞ = 0.2 m/s one can see tracks in a slightly larger wall parallel slice color coded by wall normal acceleration nicely indicating the horse shoe vortices emanating in front of the cube close to the wall. Figure 11, left-upper shows a central slice of 3 mm in thickness from a side view (60 successive time-steps are drawn). It can be seen how particles that approach the cube in low layers of the flow are being deflected by the pressure field around the cube and are transported either over the cube or into layers very close to the wall. Many of those remain close to the wall and travel around the cube at a surprisingly large radius and low velocity (see Figure 10). Large, elongated vortices are visualized by the trajectories, bent around the cube (see Figure 10 and 11 right). Separation bubbles are built at the three streamwise faces of the cube (best visible in Figure11 left up for the top face), where fluid flows backwards, until it is carried away by the suction along the sharp shear layer that is created at the edges of the cube. Here, the highest accelerations are seen (see Figure, 11 left down). Heavily turbulent flow is generated in the wake of the cube specifically for the higher laminar BL flow velocities.
Using the FlowFit algorithm, the densely tracked particles can be used in conjunction with physical regularizations to interpolate the velocity- and acceleration field onto a regular grid. As a result the temporally resolved 3D velocity and acceleration gradient tensor is available. Figure 11, right shows an instantaneous FlowFit result with iso-surfaces of vorticity. The cube is covered by connected regions of shear vorticity that quickly break up into vortices of different scales, as the flow becomes turbulent. The bent vortices surrounding the cube in upstream direction that were already visible in Figure 10, right can now be clearly identified. A large horseshoe vortex, surrounding the lower part of the cube that breaks up when secondary hairpin-type vortices are developed, is visible. Two other flow field examples visualized by 3D vorticity iso-contour surfaces of the laminar case with U_∞ = 0.8 m/s are given in Figure 12.

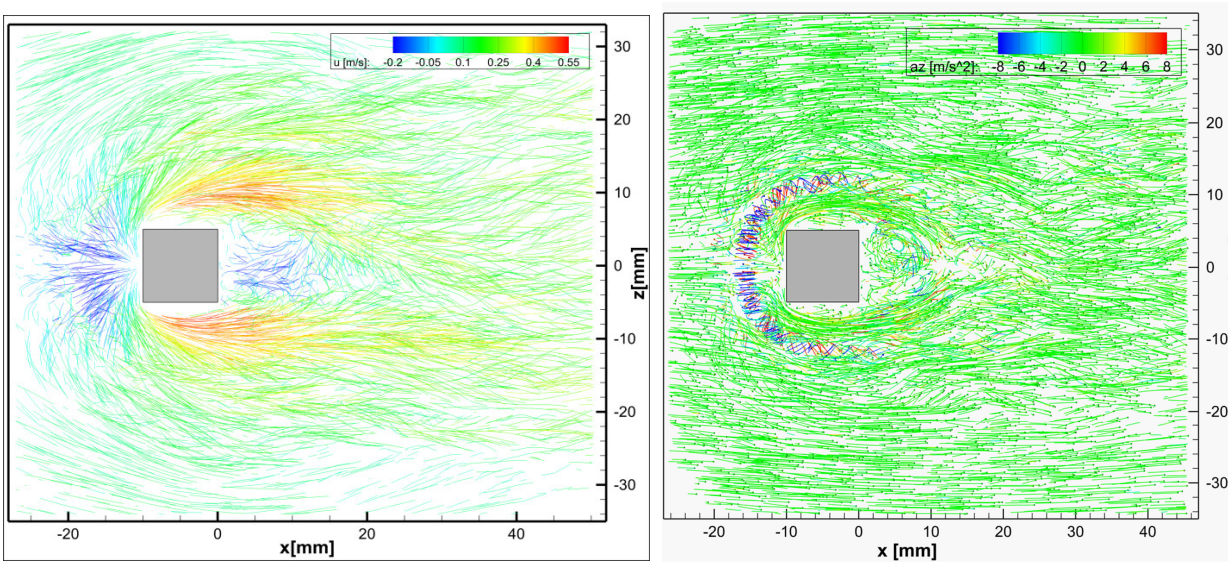

Figure 10: Left: Tracking results for U_∞ = 0.4 m/s laminar inflow, displaying a slice close to the wall (y = 0 - 1.2 mm) color-coded by streamwise velocity. Right: U_∞ = 0.2 m/s laminar inflow case with cut through volume in a slice of y = 0 – 3.5 mm and color coded by y-component of acceleration.

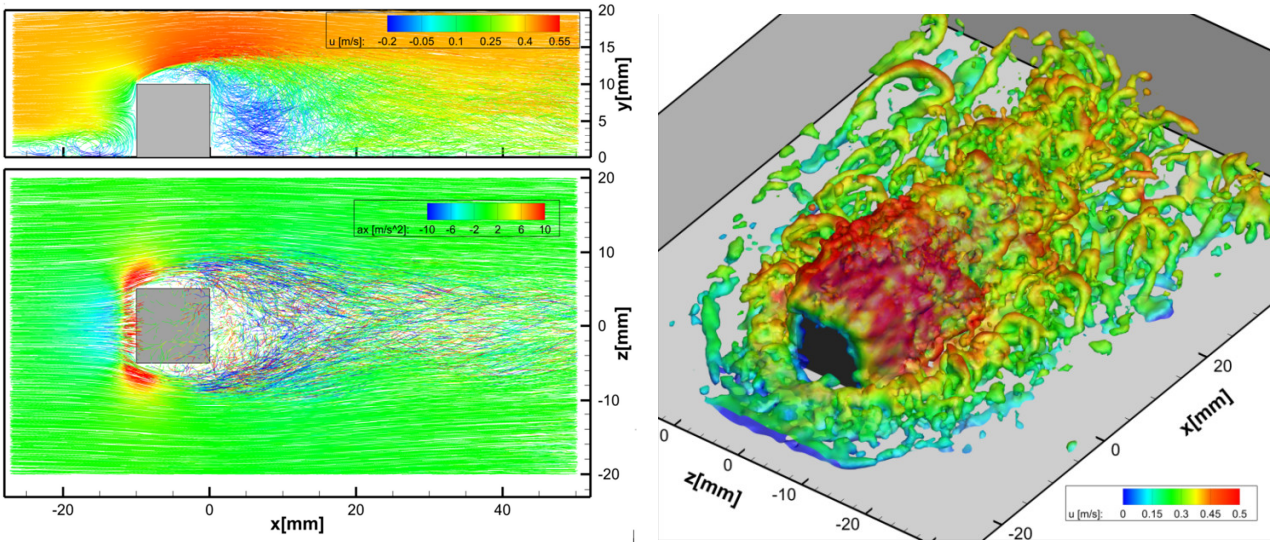

Figure 11: Tracking result for U_∞ =0.4 m/s laminar inflow. Left, top: Side view on a 3 mm slice in the middle of the cube. Particle tracks of 60 successive time-steps, color-coded by streamwise velocity. Left, bottom: View from above on a 1.3 mm slice near the top of the cube (y = 9.5 -10.8 mm), color-coded by streamwise acceleration. Right: Instantaneous snapshot of vorticity iso-surfaces (ω = 170 /s) color coded by u-velocity, as calculated by FlowFit from the STB tracking results

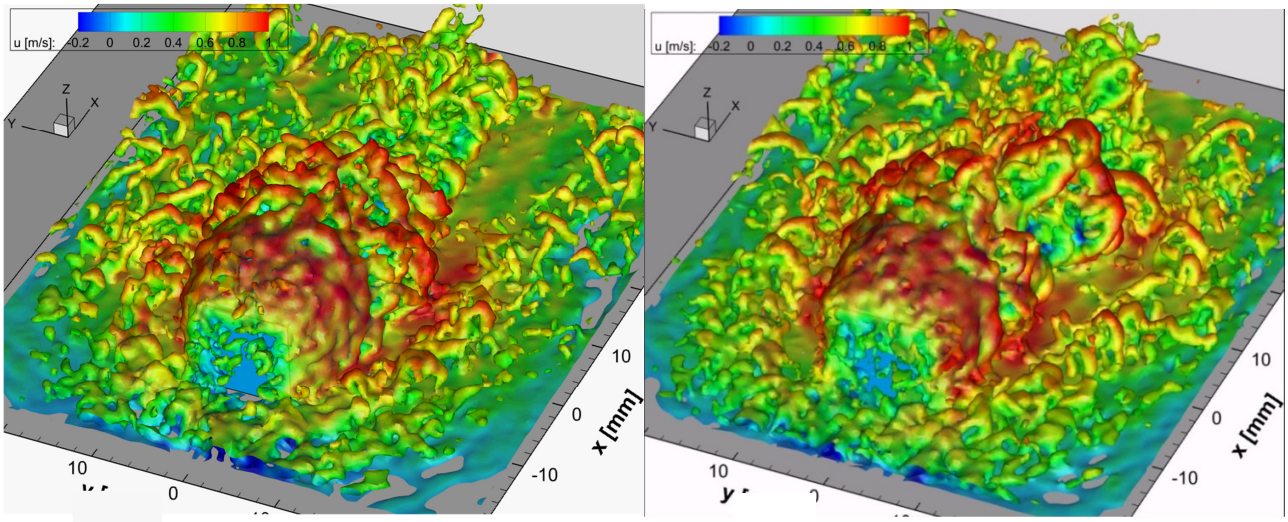

Figure 12: Two successive time-steps of U_∞ = 0.8 m/s laminar case with vorticity iso-surfaces by FlowFit.

In Fig. 12 the influence of the cube on to the stability of the laminar flow is clearly visible along the generated shear layers and the horse-shoe vortices. In all regions around and in the wake hairpin-like vortices evolve after waviness of the shear-layers and along the main vortices has been amplified. The hairpin-like vortices evolve in wall-normal and spanwise direction and are convected downstream inducing entrainment events through the wake shear layer and a spanwise growing of a turbulent wedge.

3.3. 3D Bin averaging results

A straight-forward statistical approach which preserves the high spatial resolution of the available particle tracking data while being adaptable to the threshold requirements of statistical convergences of

the different one- or multi-point statistics is the s.c. bin averaging method. Here we used all ~22,000 time steps of the tracking results to build a huge grid of 9,849,885 bins with an individual cubic bin size of 0.25^3 mm³. A result of the converged mean flow field color coded by the streamwise velocity is given in Fig. 13. Here a volumetric overview of the mean flow field given by three perpendicular cutting planes is displayed. It represents a small part of the maximal possible spatial dynamic range, which is given with the positional accuracy of the individual tracks (~0.1 px, here ~4µm) and limited only by the possible number of statistical independent samples per bin. Using symmetry conditions allow higher resolutions.

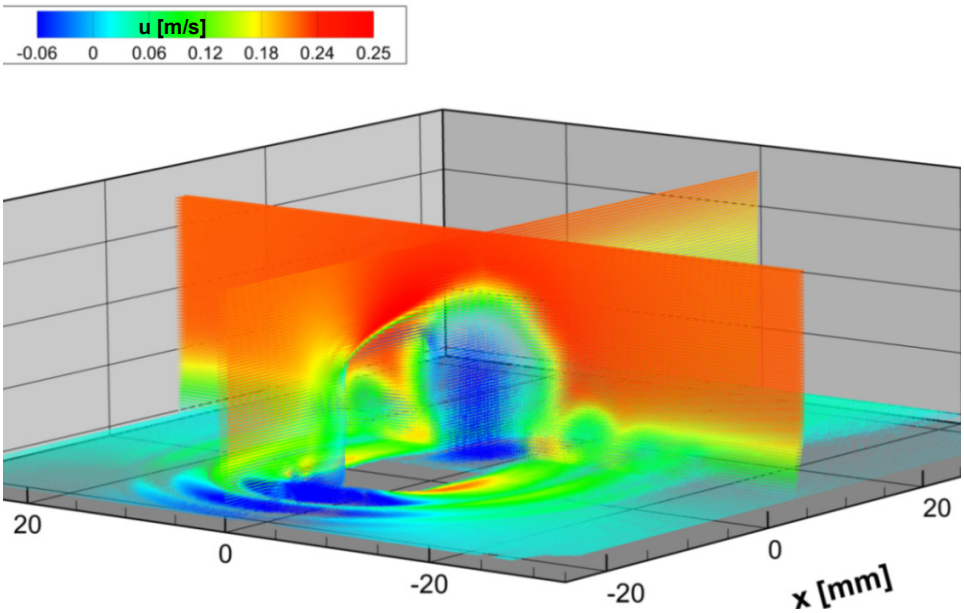

Figure 13: Result of 3D mean velocity field for the laminar BL flow case at U_∞ = 0.2 m/s based on bin-averaging approach and visualized by three perpendicular vector planes color coded by u-component of the velocity. Total of 9,849,885 volume bins of size 0.25^3 mm³

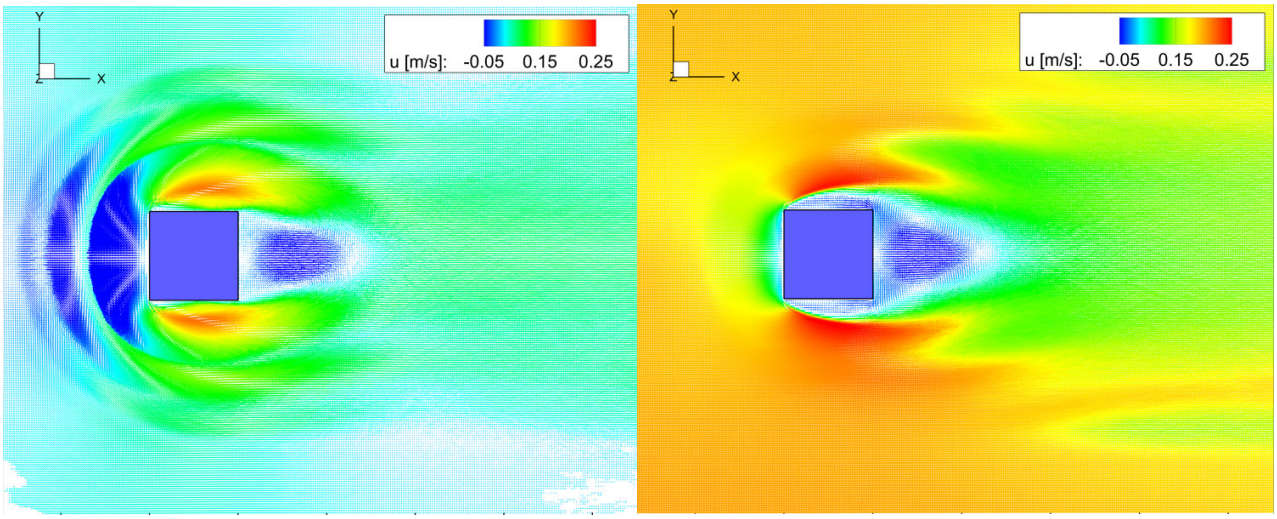

Figure 14: Result of 3D mean velocity field for laminar boundary layer flow case at U_∞ = 0.2 m/s based on bin-averaging approach (see Figure 13) and visualized by a vector plane at y = 0.5 mm (estimate of the wall-shear-stress velocity) (left) and y = 5 mm (right) both color coded by the u-component of velocity

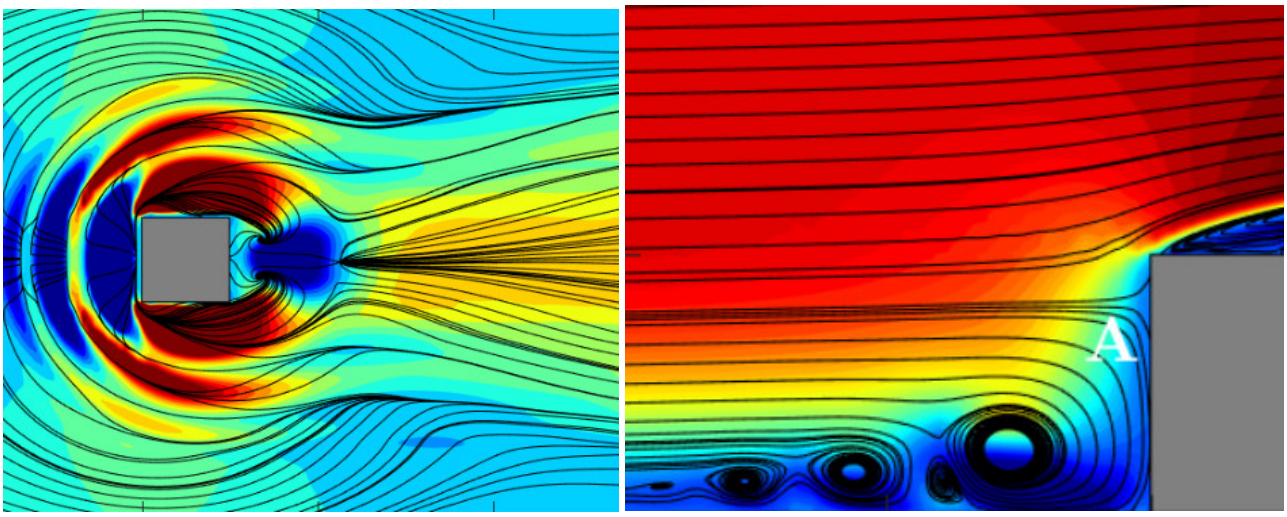

Figure 15: Results of DNS from Diaz-Daniel et al. (2017) showing mean velocity fields with streamlines for a laminar BL flow case at Re_H = 3,000 and H/δ = 1 in a plane close to the wall (left) and in the vertical center plane in front of the cube (right) both colour coded by the u-component of velocity

In figure 14 left a wall-parallel slice of the bin averaging result of Fig. 13 is given at y = 0.5 mm. For this specific case at U_∞ = 0.2 m/s or Re_H = 2,000 with H/δ = 0.42 the displayed flow structure at the wall is a good and direct approximation of the mean skin friction velocity vector distribution. The flow pattern and vector field direction of the near wall mean flow is very similar to the DNS results shown for Re_H = 3,000 in Fig. 15, left. For calculation of the overall flow induced drag the skin friction field could be integrated together with those at the surfaces of the cube itself. Such a direct estimation of the surface drag based on the flow field around an obstacle would be a very interesting novelty for aerodynamic investigations. Together with the pressure field estimation based on the same bin averaging result using the FlowFit approach in the whole volume (see Fig. 17) the classical drag estimation approach based on a wake integration of the pressure deficit can be tested and validated at different downstream wake distances with a direct comparison to the direct drag integration proposed here.

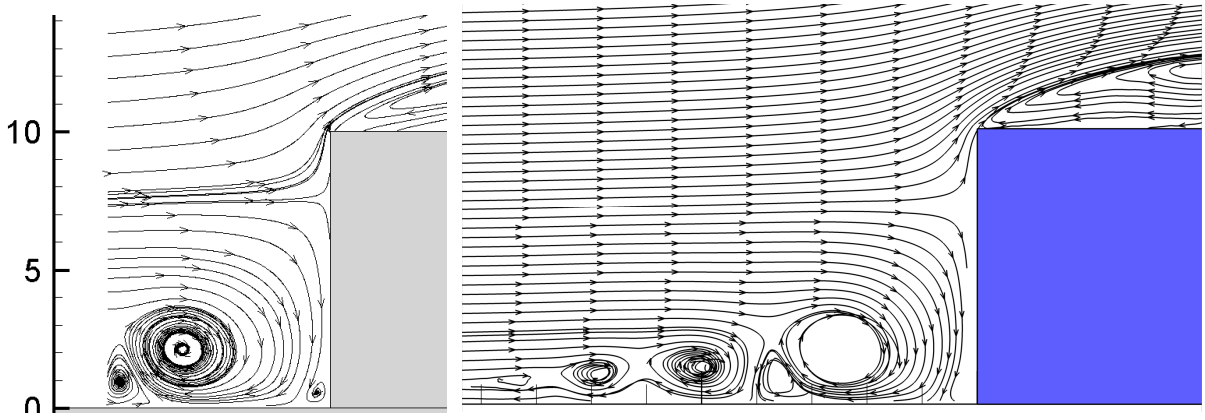

Figure 16: Stitch of two regions of the mean velocity streamlines from TR-PIV measurements for laminar boundary layer flow case at U_∞ = 0.2 m/s at z = 0 mm (left) and corresponding streamlines cut of 3D STB bin-averaging result (right)

In Fig. 16 a direct comparison of the streamlines of the 2D-2C mean velocity field from the TR-PIV measurement with the 3D bin-averaging results from the 3D STB measurement at U_∞ = 0.2 m/s in the centerplane upstream of the cube is shown. The deceleration of the flow below the cubes stagnation point

generates a hierarchy of horse-shoe vortices with negative spanwise vorticity close to the wall. In between tiny counter-rotating vortices are induced with lower vorticity values. In the 3D bin-average result the streamlines of the first-order and strongest horse-shoe vortex closest to the cubes front surface "escape" in spanwise direction (empty core) due to a small asymmetry of the averaged flow. This might be caused by the low frequency quasi-periodic oscillations in the wake downstream of the cube or by principle asymmetries of bluff-body wakes.

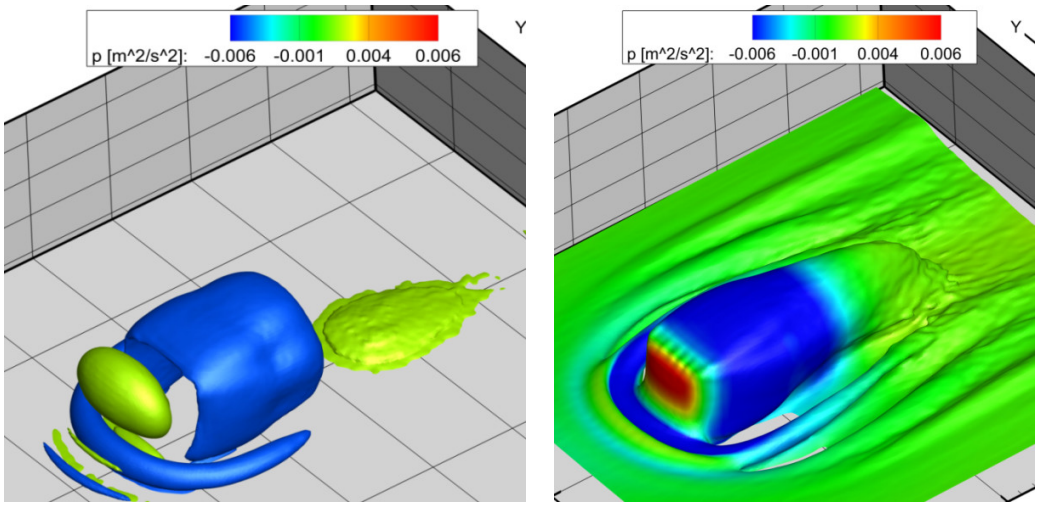

Figure 17: Mean 3D pressure field iso-surfaces around the cube based on bin-averaging (left) and the same pressure field color coded on iso-surfaces of mean u-velocity (right)

4 Conclusions

In the paper we present spatially and temporally highly resolved 2D and 3D velocity field measurements of the flow around a surface mounted cube based on TR-PIV and 3D STB. Instantaneous flow features and dynamics as well as converged flow statistics have been addressed for six Reynolds numbers at several laminar and one turbulent BL flow conditions. An experimental data base consisting of the mean velocity volumes, all corresponding six Reynolds stresses and the pressure fields of all six test cases – incoming laminar BL at U_∞ = 0.2, 0.4, 0.6 and 0.8 m/s, incoming turbulent BL at U_∞ = 0.8 m/s and clean turbulent BL (without cube) at U_∞ = 0.8 m/s complying with the standards and regulations of the ERCOFTAC data base will be prepared and transferred within the next year. Furthermore time-resolved examples of STB results using FlowFit interpolation and the pure particle trajectories can be provided after request if advanced time-resolved CFD methods (e.g. LES, DNS) see advantages for validating their codes with TR-3D flow field data. In the final data analyses and planned journal publication results from all flow cases (laminar and turbulent) will be discussed. Profiles and statistics will be compared to literature, as well as to CFD validation data that are studied in parallel of the experimental work. Instantaneous and average pressure fields, which are extracted using the FlowFit algorithm shall be further analyzed.

References

Beresh SJ, Henfling J and Spillers R (2017), "Postage-Stamp PIV:" Small Velocity Fields at 400 kHz for Turbulence Spectra Measurements, *AIAA 2017-0024, 55th AIAA Aeros. Sci. M., Grapevine, Texas*

Castro IP and Robins AG (1977), The flow around a surface-mounted cube in uniform and turbulent streams. *J. Fluid Mech.* 79 (2), 307–335

Depardon S, Lasserre JJ, Boueilh JC, Brizzi LE, and Borée J(2005), Skin friction pattern analysis using near-wall PIV. *Exp. Fluids* 39: 805–818

Diaz-Daniel C, Laizet S and Vassilicos JC (2017), Direct numerical simulations of a wall-attached cube immersed in laminar and turbulent boundary layers. *J. Heat and Fluid Flow* 68: 269–280

Gesemann S, Huhn F, Schanz D and Schröder A (2016), From noisy particle tracks to velocity, acceleration and pressure fields using B-splines and penalties. *Proc. of 18th Int. Symp. on Appl. of Laser Techniques to Fluid Mechanics, Lisbon, Portugal, 2016*

Hussein HJ and Martinuzzi RJ (1995), Energy balance for turbulent flow around a surface mounted cube placed in a channel. *Phys. Fluids* 8, 764

Iaccarino G, Ooi A, Durbin PA and Behnia M (2003), Reynolds averaged simulation of unsteady separated flow. *J. Heat and Fluid Flow* 24:147–156

Kähler CJ, Astarita T, Vlachos PP, Sakakibara J, Hain R, Discetti S, La Foy R, Cierpka C (2016), Main results of fourth International PIV-Challenge, *Exp. Fluids* 57:97

Krajnovic S and Davidson L (2002), Large-Eddy Simulation of the Flow About a Bluff Body. *AIAA J.,* 40:927–936

Martinuzzi R and Tropea C (1993), The flow around surface-mounted, prismatic obstacles placed in a fully developed channel flow. *J. Fluids Eng.* 115, 85–92.

Meinders E, Hanjalic K and Martinuzzi R (1999), Experimental study of the local convection heat transfer from a wall-mounted cube in turbulent channel flow. *J. Heat Transfer* 121 (3), 564–573

Novara M, Schanz D, Reuther N, Kähler C J and Schröder A (2016) Lagrangian 3D particle tracking in high-speed flows: Shake-The-Box for multi-pulse systems. *Exp. Fluids* 57:128

Novara M, Schanz D, Geisler R, Gesemann S, Voss C and Schröder A (2019) Multi-exposed recordings for 3D Lagrangian particle tracking with multi-pulse Shake-The-Box. *Exp. Fluids* 60:44

Schanz D, Gesemann S, Schröder A (2016) Shake-the-Box: Lagrangian particle tracking at high particle image densities. *Exp. Fluids* 57:70-97

Schanz D, Gesemann S, Schröder A, Wieneke B, Novara M (2012) Non-uniform optical transfer functions in particle imaging: calibration and application to tomographic reconstruction *Meas. Sci. Technol.* 24 024009

Schlatter P, Örlü R, Li Q, Brethouwer G, Fransson JHM, Johansson AV, Alfredsson PH and Henningson DS (2009), Turbulent boundary layers up to $Re_\theta = 2500$ studied through simulation and experiment. *Phys. Fluids* 21:051704

Schröder A, Schanz D, Novara M, Philipp F, Geisler R, Agocs J, Knopp T, Schroll M and Willert CE (2018), Investigation of a high Reynolds number turbulent boundary layer flow with adverse pressure gradients using PIV and 2D- and 3D- Shake-The-Box, *Proc. of 19th Int. Symp. on Appl. of Laser and Imaging Techniques to Fluid Mechanics, Lisbon, Portugal, 2018*

Wieneke B (2008), Volume self-calibration for 3D particle image velocimetry, *Exp. Fluids* 45, pp 549-556

Wieneke B (2013) Iterative reconstruction of volumetric particle distribution. *Meas. Sci. Technol.* 24:024008

Willert C (2015) High-speed particle image velocimetry for the efficient measurement of turbulence statistics. *Exp. Fluids* 56:17

Yakhot A, Anor T, Liu H and Nikitin N (2006a), Direct numerical simulation of turbulent flow around a wall-mounted cube: spatio-temporal evolution of large-scale vortices. *J. Fluid Mech.* 566, 1–9.

Yakhot A, Liu H and Nikitin N (2006b), Turbulent flow around a wall-mounted cube: a direct numerical simulation. *Int. J. Heat Fluid Flow* 27, 994–1009